

# Self-supervised arbitrary scale super-resolution framework for anisotropic MRI

Haonan Zhang<sup>1,\*</sup>, Yuhan Zhang<sup>1,\*</sup>, Qing Wu<sup>1</sup>, Jiangjie Wu<sup>1</sup>, Zhiming Zhen<sup>2</sup>, Feng Shi<sup>3</sup>, Jianmin Yuan<sup>4</sup>, Hongjiang Wei<sup>5</sup>, Chen Liu<sup>2,6</sup>, and Yuyao Zhang<sup>1,6</sup>

<sup>1</sup> School of Information Science and Technology, ShanghaiTech University, Shanghai, China

<sup>2</sup> Department of Radiology, Southwest Hospital, Army Medical University (Third Military Medical University), Chongqing, 400038, China

<sup>3</sup> Shanghai United Imaging Intelligence Co., Ltd., Shanghai, China

<sup>4</sup> Central Research Institute, UIH Group, Shanghai, China

<sup>5</sup> School of Biomedical Engineering, Shanghai Jiao Tong University, Shanghai, China

<sup>6</sup> Co-corresponding Authors

**Abstract.** In this paper, we propose an efficient self-supervised arbitrary-scale super-resolution (SR) framework to reconstruct isotropic magnetic resonance (MR) images from anisotropic MRI inputs without involving external training data. The proposed framework builds a training dataset using "in-the-wild" anisotropic MR volumes with arbitrary image resolution. We then formulate the 3D volume SR task as a SR problem for 2D image slices. The anisotropic volume's high-resolution (HR) plane is used to build the HR-LR image pairs for model training. We further adapt the implicit neural representation (INR) network to implement the 2D arbitrary-scale image SR model. Finally, we leverage the well-trained proposed model to up-sample the 2D LR plane extracted from the anisotropic MR volumes to their HR views. The isotropic MR volumes thus can be reconstructed by stacking and averaging the generated HR slices. Our proposed framework has two major advantages: (1) It only involves the arbitrary-resolution anisotropic MR volumes, which greatly improves the model practicality in real MR imaging scenarios (e.g., clinical brain image acquisition); (2) The INR-based SR model enables arbitrary-scale image SR from the arbitrary-resolution input image, which significantly improves model training efficiency. We perform experiments on a simulated public adult brain dataset and a real collected 7T brain dataset. The results indicate that our current framework greatly outperforms two well-known self-supervised models for anisotropic MR image SR tasks.

## 1 Introduction

Magnetic Resonance Imaging (MRI) is an essential medical imaging technology. However, isotropic 3D High-Resolution (HR) MR images are difficult to acquire due to the trade-off problem among image resolution, Signal-Noise-Ratio (SNR), and scanning time [1]. A common compromise is to scan anisotropic MR

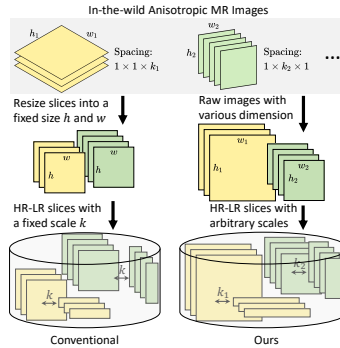


**Fig. 1.** Pipelines of building SR dataset from in-the-wild multiple anisotropic MR images. The conventional pipeline [2, 3] is to resize the raw slices into a fixed size and simulate the paired HR-LR slices of a fixed scale. While we aim to keep the slices at their raw resolutions and build the paired HR-LR slices of arbitrary scales.

images to improve SNR and shorten the scanning time. Unfortunately, the measured anisotropic MR volumes have high in-plane resolutions but low through-plane resolutions, which results in the loss of high-frequency image details in the through-plane view and may hinder the following works (e.g., lesion detection and segmentation). Thus improving the through-plane resolution to reconstruct the isotropic MR images is an urgent need for clinical medical diagnosis and research.

Currently, Convolutional Neural Networks (CNNs) are mainstream solutions for isotropic MR image Super-Resolution (SR) reconstruction. Most CNNs-based SR methods [4–7] learn inverse mappings from anisotropic inputs to isotropic outputs by training CNNs over external datasets. They produce robust and excellent SR performance benefiting from the data-driven priors. However, the fixed inverse mappings learned by CNNs suffer from severe performance drops when the up-sampling scale changes [8–10]. Therefore, an independent CNN needs to be trained in practice for each up-sampling scale. This scale-specific learning paradigm is thus extremely resource-intensive.

Recently, several arbitrary-scale MR image SR methods [11–13] based on Implicit Neural Representation (INR) have emerged. INR is a signal representation based on neural networks. The signal is formulated as a continuous function of spatial coordinates and is approximated by a Multi-Layer Perceptron (MLP). Due to the continuous representation provided by INR, the single well-trained INR-based model theoretically can handle the SR tasks of arbitrary scales and thus significantly reduce resource consumption. However, the INR-based SR methods [11–13] are almost supervised; thus, a large-scale external dataset is required for training. Moreover, scanning the isotropic 3D HR MR volumes is often time-consuming and expensive due to the trade-off problem, which significantly limits model performance and practicality.

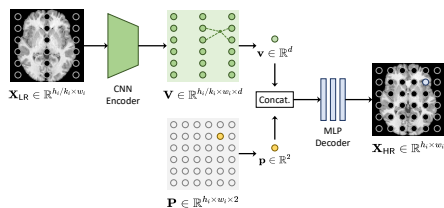


**Fig. 2.** Pipeline of our arbitrary-scale SR model.

In this work, we propose a self-supervised arbitrary-scale SR framework, in which an arbitrary-scale SR model is trained based on the multiple anisotropic MR images (Note the multiple images refer to "in-the-wild" MR volumes with arbitrary image resolution, instead of forcibly requiring anisotropic images acquired from orthogonal views.). Our single well-trained SR model can reconstruct the corresponding isotropic HR MR volumes from the multiple anisotropic inputs without involving any external training data.

To sum up, there are two major contributions in our proposed framework: (1) We propose a universal pipeline for constructing an arbitrary-resolution and arbitrary-scale SR dataset from the anisotropic MR volumes, which releases the need for external isotropic 3D HR MR images (Sec. 2.1); (2) We propose an arbitrary-scale SR model based on INR for 2D MR slices and train it on the built SR dataset (Sec. 2.2). After model training, we utilize the SR model to up-sample the 2D LR slices extracted from the anisotropic MR images along their HR views. The final isotropic volumes thus can be reconstructed by stacking and averaging the generated HR slices (Sec. 2.3).

To evaluate the proposed framework, we conduct comparison experiments on two MR image datasets (including a simulation adult dataset and a real collection fetus dataset). The results demonstrate that the proposed framework outperforms the two self-supervised methods for isotropic 3D HR MR image SR tasks while using a single-trained model to handle SR tasks of arbitrary scales.

## 2 Proposed Framework

### 2.1 Arbitrary-Resolution and -Scale SR Dataset Construction

In 2017, [2, 3] proposed a pipeline for building an SR training dataset from in-the-wild multiple anisotropic MR images. The main idea is to consider the 2D HR slices along the LR view as GT images and then perform down-sampling on the HR slices to simulate the paired 2D HR-LR slices training data. As shown in Figure 1 (Left), the conventional pipeline proposed by [2, 3] first resizes the raw HR slices into a fixed size. Then, down-sampling the HR slices by a fixed scale to simulate the corresponding LR slices. However, there are two limitations: (1) Resizing operator will cause a loss of the multi-scale information provided by the raw arbitrary-resolution HR slices; (2) The paired HR-LR slices of a fixed scale only can be used to train scale-specific SR models.

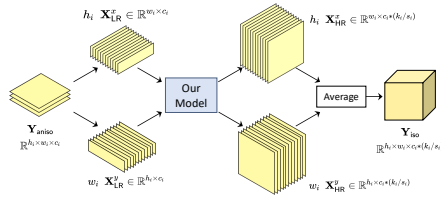


**Fig. 3.** Pipeline of an isotropic 3D HR volume reconstruction by our arbitrary-scale SR model.

Dataset	Image	Spacing (mm)	Image Size
HCP-1200 [14]	Sub #1	$1.40 \times 0.70 \times 0.70$	$130 \times 260 \times 260$
	Sub #2	$0.70 \times 1.75 \times 0.70$	$260 \times 104 \times 260$
	Sub #3	$0.70 \times 0.70 \times 2.10$	$260 \times 260 \times 87$
	Sub #4	$2.45 \times 0.70 \times 0.70$	$74 \times 260 \times 260$
	Sub #5	$0.70 \times 2.80 \times 0.70$	$260 \times 65 \times 260$
7T Adult Brain	Adult #1	$2.00 \times 0.41 \times 0.41$	$80 \times 544 \times 544$
	Adult #2	$3.00 \times 0.73 \times 0.73$	$49 \times 288 \times 288$

**Table 1.** Details of the two datasets used in our experiments.

To this end, we propose constructing an arbitrary-resolution and scale SR dataset. The pipeline is demonstrated in Figure 1 (Right). Given the measured multiple anisotropic MR volumes, we directly extract raw 2D slices along their LR views as the GT HR slices without using any resizing operator, benefiting the preserving of the original multi-resolution image information. For example, 35 slices of  $200 \times 200$  size will be extracted for an anisotropic volume of  $35 \times 200 \times 200$  size. Then, we down-sample the HR slices to simulate the corresponding 2D LR slices. Instead of the fixed scale in the conventional pipeline [2, 3], the down-sampling scales are set as the ratios between in-plane spacing and through-plan spacing in the original 3D anisotropic volumes. Finally, the generated paired HR-LR slices have arbitrary scales due to the anisotropic inputs of various spacings (i.e., voxel sizes). Therefore, our build dataset can be used for training arbitrary-scale SR models.

## 2.2 Arbitrary-Scale SR Model for 2D MR Slices

Inspired by [11], we propose an arbitrary-scale SR model for 2D MR slices. Given any pair of LR-HR images  $\{\mathbf{X}_{LR} \in \mathbb{R}^{h_i/k_i \times w_i}, \mathbf{X}_{HR} \in \mathbb{R}^{h_i \times w_i}\}$  from our arbitrary-resolution and -scale dataset, where  $k_i$  represents their up-sampling scale, we leverage a continuous function to represent them as below:

$$f_{\theta} : (\mathbf{p}, \mathbf{v}(\mathbf{p})) \rightarrow \mathbf{X}(\mathbf{p}), \quad (1)$$

where  $\mathbf{p} = (x, y) \in \mathbb{R}^2$  is any spatial coordinate in a normalized 2D Cartesian coordinates  $[-1, 1] \times [-1, 1]$ .  $\mathbf{X}(\mathbf{p}) \in \mathbb{R}$  and  $\mathbf{v}(\mathbf{p}) \in \mathbb{R}^d$  denote the intensity value and semantic representation at the position  $\mathbf{p}$  in the image  $\mathbf{X}$  respectively. The vector  $\mathbf{v}(\mathbf{p})$  is used for a conditional input such that the function  $f_{\theta}$  can be shared for different MR slices. Therefore, the paired HR-LR image  $\{\mathbf{X}_{LR}, \mathbf{X}_{HR}\}$  can be

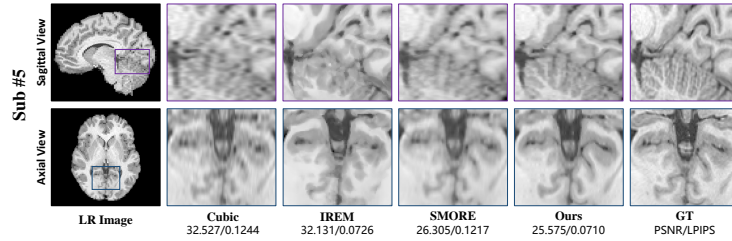


**Fig. 4.** Qualitative results of all compared methods on Sub #5 of the simulated HCP-1200 data [14] for  $4\times$  SR at coronal view.

Scale & View	Cubic	IREM [15]	SMORE [2]	Ours
$2\times$ & sagittal	39.616/0.9760/0.0297	37.632/0.9570/0.0783	41.514/0.9857/0.0259	38.928/0.9734/0.0269
$2.5\times$ & coronal	32.254/0.9499/0.0781	31.345/0.9345/0.1019	27.903/0.9061/0.0778	31.038/0.9510/0.0518
$3\times$ & axial	36.764/0.9702/0.0718	34.889/0.9523/0.0632	32.749/0.9470/0.0757	32.255/0.9719/0.0286
$3.5\times$ & sagittal	25.568/0.8904/0.1398	25.370/0.8813/0.1004	21.320/0.8541/0.1436	25.064/0.8857/0.0781
$4\times$ & coronal	32.527/0.9244/0.1244	32.131/0.9181/0.0726	26.305/0.8619/0.1217	25.575/0.9144/0.0710
<b>Mean</b>	33.346/0.9422/0.0888	32.273/0.9286/0.0833	29.958/0.9110/0.0889	30.572/0.9393/0.0513

**Table 2.** Quantitative results (PSNR/SSIM/LPIPS) of all compared methods on the simulated HCP-1200 data [14].

considered as the discrete explicit representation of the continuous function  $f_\theta$  at different sampling spacing.

Based on the definition above, the arbitrary-scale SR task is converted to learn the continuous function  $f_\theta$ . Figure 2 shows the pipeline. We first employ a CNN encoder  $\mathcal{C}_\phi$  to map the LR image  $\mathbf{X}_{LR}$  to a feature map  $\mathbf{V} \in \mathbb{R}^{h_i/k_i \times w_i \times d}$ , where an element  $\mathbf{v}$  is the local semantic representation of the input image  $\mathbf{X}_{LR}$ . Then, for a query coordinate  $\mathbf{p}$  in HR grid  $\mathbf{P} \in \mathbb{R}^{h_i \times w_i \times 2}$  built on the HR image  $\mathbf{X}_{HR}$ , we generate the corresponding feature vector  $\mathbf{v}(\mathbf{p})$  by performing linear interpolation on the feature map  $\mathbf{V}$ . Then, the vector  $\mathbf{v}(\mathbf{p})$  as a conditional input that concatenated with the coordinate  $\mathbf{p}$  is feed into a Multi-Layer Perceptron (MLP) decoder  $\mathcal{M}_\psi$  to predict the HR intensity value  $\hat{\mathbf{X}}_{HR}(\mathbf{p})$ . Finally, we simultaneously optimize the CNN encoder and MLP decoder to learn the function by minimizing the objective as below:

$$\phi^*, \psi^* = \arg \min_{\phi, \psi} \mathcal{L}(\mathbf{X}_{HR}(\mathbf{p}), \hat{\mathbf{X}}_{HR}(\mathbf{p})), \quad (2)$$

$$\hat{\mathbf{X}}_{HR}(\mathbf{p}) = \mathcal{M}_\psi(\mathbf{p}, \mathbf{v}(\mathbf{p})), \quad (3)$$

$$\mathbf{v}(\mathbf{p}) = \text{Linear Inter.}(\mathbf{V}), \quad (4)$$

$$\mathbf{V} = \mathcal{C}_\phi(\mathbf{X}_{LR}), \quad (5)$$

where the loss function  $\mathcal{L}$  is implemented by  $\ell_1$  norm. We use Adam optimizer to train the model, and its hyper-parameters are default. The initial learning rate is  $1e-4$ , and the training epoch is 800. The best model is saved by checkpoints during the training process.

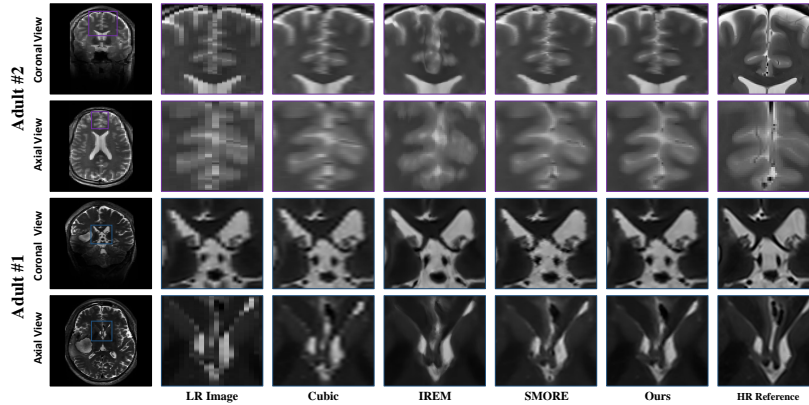


Fig. 5. Qualitative results of all compared methods on the two samples of the real 7T adult brain data for  $4.86\times$  and  $4.11\times$  SR at sagittal view.

### 2.3 Isotropic 3D HR Volumes Reconstruction

Figure 3 illustrates the pipeline of an isotropic 3D HR volume reconstruction by our well-trained model. Let  $\mathbf{Y}_{\text{aniso}} \in \mathbb{R}^{h_i \times w_i \times c_i}$  of a spacing  $s_i \times s_i \times k_i$  ( $s_i < k_i$ ) denote any one of the anisotropic input volumes, our purpose is to recover the corresponding isotropic image  $\mathbf{Y}_{\text{iso}}$  of a spacing  $s_i \times s_i \times s_i$  by using the well-trained ArSSR2D model. To this end, we first extract  $h_i$  LR slices  $\mathbf{X}_{\text{LR}}^x \in \mathbb{R}^{w_i \times c_i}$  and  $w_i$  LR slices  $\mathbf{X}_{\text{LR}}^y \in \mathbb{R}^{h_i \times c_i}$  from  $\mathbf{Y}_{\text{aniso}}$  along two HR views, respectively. Then, these LR slices are fed our SR model to generate their HR versions, i.e.,  $h_i$   $\mathbf{X}_{\text{HR}}^x \in \mathbb{R}^{w_i \times c_i * (k_i/s_i)}$  and  $w_i$   $\mathbf{X}_{\text{HR}}^y \in \mathbb{R}^{h_i \times c_i * (k_i/s_i)}$ . Finally, we can reconstruct the isotropic volume  $\mathbf{Y}_{\text{iso}} \in \mathbb{R}^{h_i \times w_i \times c_i * (k_i/s_i)}$  by stacking and averaging the generated HR slices.

## 3 Experiments

### 3.1 Experimental Setup

**Simulated HCP-1200 Data:** HCP-1200 dataset [14] is a large-scale public adult brain MR image dataset consisting of 1113 3D isotropic HR multi-modal brain MR images. In our experiments, we use five isotropic HR T1-weighted MR images of the HCP-1200 dataset [14] as Ground Truth (GT) images. To simulate anisotropic LR input images, we then respectively downsample the five GT images by the scales  $\{2, 2.5, 3, 3.5, 4\}$  along the  $\{x, y, z, x, y\}$  views, where  $x$ ,  $y$ , and  $z$  denote respectively sagittal, coronal, and axial views. The GT images are only used for final model evaluation, while all the compared models do not see them during the model training.

**Real 7T Adult Brain Data:** We scan two T2-weighted anisotropic brain MR images from two adults *in vitro* on a 7T Siemens MR scanner. The spacing of the

raw images are  $2 \times 0.4118 \times 0.4118$  mm and  $3 \times 0.2431 \times 0.2431$  mm respectively. The size of the raw images are  $80 \times 544 \times 544$  and  $49 \times 864 \times 864$  respectively. To reduce computational consumption while maintaining image content as much as possible, we decrease the latter size to  $49 \times 288 \times 288$  by cropping.

**Compared Methods:** We compare our model with three SR methods: (1) Cubic interpolation, a mathematical method based on cubic polynomials; (2) IREM, a self-supervised SR method based on INR. (3) SMORE [2], a deep learning method based on self super-resolution (SRR) [16]. Here Cubic interpolation is based on the scikit-image library of Python, while IREM [15] and SMORE [2] are reproduced following the original papers.

**Evaluation Metrics:** PSNR and SSIM [17], two widely-used image quality evaluation metrics, are computed. Moreover, we also calculate LPIPS [18], a popular deep-learning-based similarity metric for a more comprehensive evaluation. The slice-by-slice strategy is employed to calculate LPIPS [18] since it is designed for 2D images. Specifically, we first extract the most central 30 2D slices from SR volumes along three orthogonal views (i.e., ten images per view). Then, we calculate LPIPS [18] based on the 2D slices and average them to obtain the final scores.

### 3.2 Results on Simulated HCP-1200 Data

We compare our proposed method with the three baselines based on the five simulated anisotropic MR volumes (details in Table 1) of the HCP-1200 dataset [14]. Specifically, we apply the four methods to upsample the five anisotropic adult brain images to generate the corresponding isotropic volumes. It is worth noting that IREM [15] and SMORE [2] are independently trained for each input volume, while our single well-trained model is shared for the five different volumes.

Figure 4 shows the qualitative results on Sub #5 for the  $4 \times$  SR task at the coronal view. Cubic interpolation produces a very blurry SR image. IREM [15] yields an overly smooth image. The SR result from SMORE [2] is excellent in image structure but unclear in image details. In comparison, the SR image of our method is closest to GT in both image sharpness and consistency. Moreover, Figure 4 shows an interesting result: although the SR result by cubic interpolation is worst from the visualization, it obtains the highest PSNR (32.527 dB). As claimed in [7, 19], we hold that, the PSNR metric is defined on pixel-by-pixel distance and thus is limited for evaluating SR tasks. Instead, LPIPS [18] is measured based on semantic representations extracted by a pre-trained deep learning model. For Sub #5, our model obtains the best performance (0.071) in terms of LPIPS, which is consistent with our visual observation. We also report the quantitative results in Table 2. We observe that cubic interpolation yields the highest PSNR and SSIM (33.346 dB and 0.9422), while our proposed method obtains the best performance (0.0515) in LPIPS.

### 3.3 Results on Real 7T Adult Brain Data

Although our proposed framework yields significant improvements on the simulated HCP-1200 data [14] compared with the three baselines, it is more important to show how well the models perform on the real acquired anisotropic MR volumes. Therefore, we also conducted a comparison experiment on two real measured anisotropic adult brain volumes (details in Table 1). Here we only report the qualitative results since the isotropic GT HR images are not acquired.

As shown in Figure 5, the SR results of cubic interpolation suffer from severe blocking artifacts due to its poor de-aliasing ability. While IREM [15] produces sharp but overly smooth MR images, where many high-frequency details are lost. In comparison, the SR results of SMORE [2] and our proposed model recover more image details. Moreover, the SR results of our model are better in terms of anatomical consistency.

## 4 Conclusion

This work presents a self-supervised deep-learning framework to reconstruct the isotropic volumes from multiple anisotropic MR images when without any extra data. In the proposed framework, we first construct an arbitrary-scale SR dataset based on the anisotropic volumes, then train an arbitrary-scale SR model on our built dataset. The well-trained single SR model can be used to reconstruct the HR isotropic MR images. The experimental results on the simulated HCP-1200 [14] data and the real 7T adult brain data indicate that our proposed method can recover excellent HR isotropic MR images. Our proposed self-supervised framework has great application potential for improving MR image quality.

## 5 Compliance with ethical standards

This study was performed in line with the principles of the Declaration of Helsinki. Approval was granted by the Ethics Committee of the Southwest hospital, Chongqing, China.

## 6 Acknowledgments

This work is supported by the National Natural Science Foundation of China (No. 62071299, 61901256, 91949120).

## References

1. Yuanyuan Jia, Ali Gholipour, Zhongshi He, and Simon K Warfield, “A new sparse representation framework for reconstruction of an isotropic high spatial resolution mr volume from orthogonal anisotropic resolution scans,” *IEEE transactions on medical imaging*, vol. 36, no. 5, pp. 1182–1193, 2017.

2. Can Zhao, Aaron Carass, Blake E. Dewey, and Jerry L. Prince, “Self super-resolution for magnetic resonance images using deep networks,” in *2018 IEEE 15th International Symposium on Biomedical Imaging (ISBI 2018)*, 2018, pp. 365–368.
3. Martin Weigert, Loic Royer, Florian Jug, and Gene Myers, “Isotropic reconstruction of 3d fluorescence microscopy images using convolutional neural networks,” in *International Conference on Medical Image Computing and Computer-Assisted Intervention*. Springer, 2017, pp. 126–134.
4. Chi-Hieu Pham, Aurélien Ducournau, Ronan Fablet, and François Rousseau, “Brain mri super-resolution using deep 3d convolutional networks,” in *2017 IEEE 14th International Symposium on Biomedical Imaging (ISBI 2017)*. IEEE, 2017, pp. 197–200.
5. Yuhua Chen, Yibin Xie, Zhengwei Zhou, Feng Shi, Anthony G Christodoulou, and Debiao Li, “Brain mri super resolution using 3d deep densely connected neural networks,” in *2018 IEEE 15th International Symposium on Biomedical Imaging (ISBI 2018)*. IEEE, 2018, pp. 739–742.
6. Jinglong Du, Zhongshi He, Lulu Wang, Ali Gholipour, Zexun Zhou, Dingding Chen, and Yuanyuan Jia, “Super-resolution reconstruction of single anisotropic 3d mr images using residual convolutional neural network,” *Neurocomputing*, vol. 392, pp. 209–220, 2020.
7. Yuhua Chen, Feng Shi, Anthony G Christodoulou, Yibin Xie, Zhengwei Zhou, and Debiao Li, “Efficient and accurate mri super-resolution using a generative adversarial network and 3d multi-level densely connected network,” in *International Conference on Medical Image Computing and Computer-Assisted Intervention*. Springer, 2018, pp. 91–99.
8. Jiwon Kim, Jung Kwon Lee, and Kyoung Mu Lee, “Accurate image super-resolution using very deep convolutional networks,” in *Proceedings of the IEEE conference on computer vision and pattern recognition*, 2016, pp. 1646–1654.
9. Xuecai Hu, Haoyuan Mu, Xiangyu Zhang, Zilei Wang, Tieniu Tan, and Jian Sun, “Meta-sr: A magnification-arbitrary network for super-resolution,” in *Proceedings of the IEEE/CVF conference on computer vision and pattern recognition*, 2019, pp. 1575–1584.
10. Yinbo Chen, Sifei Liu, and Xiaolong Wang, “Learning continuous image representation with local implicit image function,” in *Proceedings of the IEEE/CVF conference on computer vision and pattern recognition*, 2021, pp. 8628–8638.
11. Qing Wu, Yuwei Li, Yawen Sun, Yan Zhou, Hongjiang Wei, Jingyi Yu, and Yuyao Zhang, “An arbitrary scale super-resolution approach for 3-dimensional magnetic resonance image using implicit neural representation,” *arXiv preprint arXiv:2110.14476*, 2021.
12. Xin Wang, Kai Xuan, Sheng Wang, Honglin Xiong, Lichi Zhang, and Qian Wang, “Arbitrary reduction of mri slice spacing based on local-aware implicit representation,” *arXiv preprint arXiv:2205.11346*, 2022.
13. Dave Van Veen, Rogier Van der Sluijs, Batu Ozturkler, Arjun Desai, Christian Bluethgen, Robert D Boutin, Marc H Willis, Gordon Wetzstein, David Lindell, Shreyas Vasanawala, et al., “Scale-agnostic super-resolution in mri using feature-based coordinate networks,” *arXiv preprint arXiv:2210.08676*, 2022.
14. David C Van Essen, Stephen M Smith, Deanna M Barch, Timothy EJ Behrens, Essa Yacoub, Kamil Ugurbil, Wu-Minn HCP Consortium, et al., “The wu-minn human connectome project: an overview,” *Neuroimage*, vol. 80, pp. 62–79, 2013.

15. Qing Wu, Yuwei Li, Lan Xu, Ruiming Feng, Hongjiang Wei, Qing Yang, Boliang Yu, Xiaozhao Liu, Jingyi Yu, and Yuyao Zhang, “Irem: High-resolution magnetic resonance image reconstruction via implicit neural representation,” in *International Conference on Medical Image Computing and Computer-Assisted Intervention*. Springer, 2021, pp. 65–74.
16. Can Zhao, Aaron Carass, Blake E. Dewey, and Jerry L. Prince, “Self super-resolution for magnetic resonance images using deep networks,” in *2018 IEEE 15th International Symposium on Biomedical Imaging (ISBI 2018)*, 2018, pp. 365–368.
17. Zhou Wang, Alan C Bovik, Hamid R Sheikh, and Eero P Simoncelli, “Image quality assessment: from error visibility to structural similarity,” *IEEE transactions on image processing*, vol. 13, no. 4, pp. 600–612, 2004.
18. Richard Zhang, Phillip Isola, Alexei A Efros, Eli Shechtman, and Oliver Wang, “The unreasonable effectiveness of deep features as a perceptual metric,” in *Proceedings of the IEEE conference on computer vision and pattern recognition*, 2018, pp. 586–595.
19. Jiancong Wang, Yuhua Chen, Yifan Wu, Jianbo Shi, and James Gee, “Enhanced generative adversarial network for 3d brain mri super-resolution,” in *Proceedings of the IEEE/CVF Winter Conference on Applications of Computer Vision*, 2020, pp. 3627–3636.